Research Article
Theoretical Study and Estimation of Recombination Rate and Photocurrent of Quantum Dot Solar Cell using Homotopy Analysis

[1]B. Murali Babu, [2]M. Madheswaran and [3]K.R. Kavitha
[1]Department of Electrical and Electronics Engineering, Paavai Engineering College, Namakkal-637 018,
[2]Centre for Advanced Research, Mahendra Engineering College, Mallasamudram-637 503,
[3]Department of Electronics and Communication Engineering, Sona College of Technology,
Salem-636005, Tamil Nadu, India

Abstract: The objective of this study is to develop the numerical model of InGaAs QD solar cell to describe the device characteristics. The developed model is based on Homotopy analysis which provides self-consistent and nonlinear solutions to 3D Poisson and Schrodinger equations. The exact potential and energy profile of the quantum dot accounts for the estimation of current under dark condition. The model is used in photocurrent determination of quantum dot solar cell under 1 Sun, 1.5 AM condition over a range of various solar cell parameters such as optical generation life time, quantum dot concentration and number of quantum dot layer. The quantum wavelength and quantum dot layers are used to calculate the photocurrent, recombination rate and conversion efficiency. The photocurrent has achieved its superiority with optimum quantum dot layers and wavelength. The results obtained show that the photocurrent is strongly sensitive to the above dependences and a good agreement with the experimental results was evidenced.

Keywords: Homotopy analysis, poisson equation, quantum dot, schrodinger equation, solar cell

INTRODUCTION

Photovoltaics have reached a tremendous growth during last two decades and power generation using photovoltaics plays a dominant role in addressing the future electricity needs of about 30 TW, in spite of the robust growth of nuclear and wind energy. The photovoltaic conversion of the fraction of 1.2×10^{25} TW of energy from sun's solar radiation contributes to the present and future energy needs. This enormously increases the interest of understanding quantum nano structures in solar cells. These preconditions envisioned the technological revolution and advancements in the nanotechnology devices such as Quantum well, Quantum Dot (QD) and Quantum wires. The photovoltaic technology based on materials with large cost/watts lead to third generation photovoltaics with significant lower cost and increased efficiency to the actual values. The increase in energy gaps with shrinking dimensions, strong photoluminescence, multiple exciton generations and relaxation of excited carriers realized the use of quantum dots in solar cell structures.

QDs are semiconductor nano particles, having unique properties such as narrow emission peak, broad excitation range and size dependent emission wavelength in which excitons are confined in all the three spatial dimensions. Fonseca *et al*. (1998) realized the confinement by fabricating the semiconductor in very small size and found QDs act like artificial atoms, showing controllable discrete energy levels. Sheng and Leburton (2002) modeled the vertically stacked and coupled InAs/GaAs Self-Assembled quantum Dots (SADs). It showed the strong hole localization and a non-parabolic dependence of the inter band transition energy on the electric field. It was reported that, the 3D strain field causes the anomalous quantum confined stark effect.

Three-dimensional spin-qubit quantum dot devices were modeled by Melnikov *et al*. (2005). The electronic properties of the devices based on double and triple quantum dots were studied numerically. Battacharya *et al*. (2002) presented the electrical and optical characteristics of self-organized QDs grown by molecular beam epitaxy. The importance of performing self-consistent calculations of Poisson equations was discussed by Datta (2000) and the V-I characteristics of nano scale structures were determined depending on the quantum transport mechanism.

QD solar cells have the potential to improve the efficiency for solar energy conversation by utilizing the additional photocurrent generated in QDs inserted in the intrinsic region of the structure. Milicic *et al*. (2000) discussed the placing of QDs to provide high absorption

Corresponding Author: B. MuraliBabu, Department of Electrical and Electronics Engineering, Paavai Engineering College, Namakkal-637 018, Tamil Nadu, India

coefficient. QD spacing and dot density play the role of additional generation or recombination centers. Aroutiounian *et al*. (2001) incorporated QDs with two counteracting effects of short circuit current and open circuit voltage.

Al-Daby *et al*. (2010) developed a 3D mathematical model based on green function to evaluate the spectral response and optimization of parameters like cell thickness, grain size and boundary recombination velocity. Semichaevsky and Johnson (2013) presented the semi classical and quantum mechanical model for carrier transport in p-i-n quantum dot solar cell. The model combined the Boltzmann-Fokker-Planck and density formalisms. The absorption of photons with energies less than the bulk GaAs band gap and stacked layers of quantum dot layers with high-in-plane densities contributed to the photocurrent. The photocurrent depended on the QD density, morphology and defect density by considering the quantum scattering.

Marti *et al*. (2001) reviewed the design constraints of quantum dot intermediate band solar cell and reported the reduction of efficiency to 46% due to recombination in barrier region. Aly and Nasr (2014) investigated and studied the role of inter-bands between the valence and conduction bands in solar cells. The time dependent Schrodinger equation was used to determine the optimum width and location of the intermediate band. The achievement of maximum efficiency by changing the width of the quantum dots and barrier distance was studied.

Nasr (2013) investigated the QD Solar Cells (QDSCs) and determined the dependence of photocurrent on its various solar parameters and the spectral response was theoretically calculated. The obtained results ensure that an enhancement of conversion efficiency upto 73% in consequence of intrinsic region in the p-n junction was equipped by QD layers. The maximum photocurrent was obtained for wavelength around 200 nm. Eshaghi Gorji *et al*. (2012) studied the inter band transition rate and surface recombination rate of carriers in QDs of intermediate band solar cells to optimize its photocurrent and efficiency. The calculation and formulation of these rates were done at two different recombination life times and the photocurrent and efficiency of solar cell were enhanced.

The available literatures demonstrate the potential of QD solar cell in solar energy conversion. The several methods used in literatures to model the QD solar cell did not focus on the real time solutions for numerical modeling and include quantum mechanical effects. The literatures did not look deep into the electron dynamics of semiconductor quantum dot solar cell. This lead to the realistic search and deep understanding of nanometer scale semiconductor physics in QD solar cell. The modeling methods discussed does not paid

much attention in validating with experimental results and provide any alternate solutions to nonlinear problems.

Hossein Zadeh *et al*. (2010) have solved many integral equations using homotopy analysis. A comparison of solutions shows that the homotopy analysis was very effective and convenient for solving integral and integro-differential equations. Yildirim (2008) has calculated the exact and numerical solutions of Poisson equation for electrostatic potential problems. The exact solutions of electrostatic potential problems defined by Poisson equation were calculated using homotopy perturbation method and boundary element method. The comparisons between these two methods were presented. Fariborzi and Fallahzadeh (2012) solved the linear and nonlinear Schrodinger equations based on the Homotopy Analysis Method (HAM). The exact solution of linear or nonlinear Schrodinger equation was obtained using convergence theorems.

Keeping the above facts and consideration, the present research work is focused on numerical modeling of QD solar cell in 3D using Homotopy analysis method. The obtained device and solar parameters of the QD solar cell using the Homotopy analysis are discussed. The Homotopy analysis is found to provide efficient and self-consistent solutions for the boundary value problems and found to be accurate, fast, flexible and reliable and provides alternate solution to nonlinear problems. The results obtained show that the photocurrent is strongly influenced by the QD and solar parameters and a good agreement with the experimental results is found and it exhibits the validity of the proposed model.

METHODOLOGY

The QD solar cell consists of a multi-stacked InGaAs layers separated by wide band-gap material GaAs. The generalized structural view of the InGaAs QD solar cell is shown in Fig. 1. When sunlight is incident on the basic structure, electron-hole pairs are generated inside the p-i-n junction region. The closely spaced QDs form the intermediate band and absorb photons of energy less than the band gap of barrier through the confined states in the dot material. Each layer has identical QDs in the active region with density e_{QD} and it reduces the dark current due to its large lateral size with bound states. It absorbs the photon in larger wavelength spectrum and photogenerated carriers are created, when an electron from the valence band is excited into the conduction band by absorption of photons with energy greater than the band gap. These excited carriers are at non-equilibrium state and they collide freely or return to equilibrium state by carrier recombination.

Similarly, the existence of single energy level of QD solar cell is provided by small transverse length L
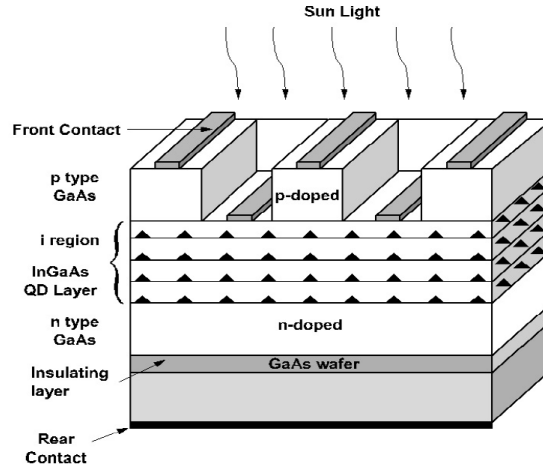
Fig. 1: Structural view of the QD solar cell

of QD, which is associated with the quantization in this direction and it is small compared with the QD spacing S. The QDs in solar cell increases the short circuit current and decreases the open circuit voltage. The structure plays the role of active region which is sandwiched between two heavily doped regions and these regions serve as front and rear contacts. The energy transition occurs from valence band to conduction band in the QD layer.

The current arising during applied voltage is determined by the potential distribution in the QD active region. The electric potential in the QD layer is equal to the sum of the average potential created by all the QDs and donors at plane z = L. The distribution of electric potential in the active region is governed by the Poisson Eq. (1), where space charge is averaged in the in-plane direction:

$$\left(\frac{\partial^2}{\partial x^2} + \frac{\partial^2}{\partial y^2} + \frac{\partial^2}{\partial z^2}\right)\varphi = -\frac{4\pi q}{\epsilon}\left[e_{QD}\langle N\rangle\sum_{i,j,k}\delta(x-x_i)\delta(y-y_j)\delta(z-z_k) - \sigma_D\right]$$ (1)

where,
ε = The dielectric constant
q = The electron charge
i, j, k = The in-plane coordinates
e_{QD} = The density of the QD
N = The number of electrons in QD layer
δ = The Dirac delta function
QD = The donor concentration

$\delta(x), \delta(y)$ and $\delta(z)$ are the QD form factors in lateral and growth directions, x_i, y_j are the QD coordinates and z_k corresponds to the growth direction. The injected current is controlled by barrier potential and the barrier is formed by the charges of electrons in QD layer, charges of remote QDs and donors. The height of barrier potential is maximum in the QD and minimum between them. The minimum height known

as punctures through which most of the injected current flows is obtained by solving the Eq. (1) through the boundary condition:

$$\varphi\mid_{z=0} = 0 \text{ -Emitter end and } \varphi\mid_{z=(U+1)L} = V$$
-Collector end (2)

V is the applied voltage and $(U + 1)L$ is the width of the active region. Averaging in the lateral direction, the Eq. (1) becomes:

$$\frac{\partial^2\varphi}{\partial z^2} = \frac{4\pi e}{\epsilon}\left[e_{QD}\langle N\rangle\sum_k\delta(z-z_k) - \sigma_D\right]$$ (3)

$z_k = uL$ is the index of the kth QD layer, u = 1, 2, 3, 4.....U and U is the number of QD layer, L is the length of the QD layer. Equation (3) can be rewritten as:

$$\frac{\partial^2\varphi}{\partial z^2} = \frac{4\pi e}{\epsilon}\left[e_{QD}\langle N\rangle\sum_{u=1}^{U}\delta(z-uL) - \sigma_D\right]$$ (4)

The surface potential of the QD using Homotopy analysis method (Madheswaran and Kavitha, 2013) is used for the estimation of solar cell parameters. Consider the initial condition as φ (x, y, 0) = 0, the Eq. (4) can be rewritten as:

$$R(\mu_0) = \frac{\partial^2\varphi_0}{\partial z^2} - \frac{4\pi e}{\epsilon}\left[e_{QD}\langle N\rangle\sum_{u=1}^{U}\delta(z-uL) - \sigma_D\right]$$ (5)

where,
$R(\mu)$: The homotopy parameter
$R(\mu_0)$: The initial guess of $R(\mu)$

Thus as the homotopy parameter increases from 0 to 1, φ_0 varies continuously to φ_1. Such variation is called deformation in topology. So the first order deformation equation can be written as:

$$\varphi_1 = \iint R(\mu_0) \, dz^2 \tag{6}$$

Substituting the value of $R(\mu_0)$ in Eq. (5), the value of φ_1 becomes:

$$\varphi_1 = -\frac{4\pi e}{\epsilon} \left[e_{QD} \langle N \rangle Uz - \sigma_D \frac{Z^2}{2} \right] \tag{7}$$

The second homotopy parameter $R(\mu_1)$ can be written as:

$$R(\mu_1) = \frac{\partial^2}{\partial z^2} [\varphi_1] - \frac{4\pi e}{\epsilon} \left[e_{QD} \langle N \rangle \sum_{u=1}^{U} \delta(z - uL - \sigma D) \right] \tag{8}$$

Substituting the value of φ_1 in Eq. (8), the $R(\mu_1)$ becomes:

$$R(\mu_1) = \frac{\partial^2}{\partial z^2} \left[-\frac{4\pi e}{\epsilon} \left[e_{QD} \langle N \rangle Uz - \sigma_D \frac{Z^2}{2} \right] - \frac{4\pi e}{\epsilon} \left[e_{QD} \langle N \rangle \sum_{u=1}^{U} \delta(z - uL) - \sigma_D \right] \right] \tag{9}$$

The second order deformation equation can be written as:

$$\varphi_2 = \iint R(\mu_1) \, dz^2 \tag{10}$$

Substituting the value of $R(\mu_1)$ in Eq. (10), the value of φ_2 becomes:

$$\varphi_2 = \frac{4\pi e}{\epsilon} \sigma_D \frac{Z^2}{2} - \frac{4\pi e}{\epsilon} e_{QD} \langle N \rangle Uz + \frac{4\pi e}{\epsilon} \sigma_D \frac{Z^2}{2} \tag{11}$$

The third homotopy parameter $R(\mu_2)$ can be written as:

$$R(\mu_2) = \frac{\partial^2}{\partial z^2} [\varphi_2] - \frac{4\pi e}{\epsilon} \left[e_{QD} \langle N \rangle \sum_{u=1}^{U} \delta(z - uL - \sigma D) \right] \tag{12}$$

Substituting the value of φ_2 in Eq. (12), the $R(\mu_2)$ becomes:

$$R(\mu_2) = \frac{\partial^2}{\partial z^2} \left[\frac{8\pi e}{\epsilon} \sigma_D \frac{Z^2}{2} - \frac{4\pi e}{\epsilon} e_{QD} \langle N \rangle Uz \right] - \frac{4\pi e}{\epsilon} \left[e_{QD} \langle N \rangle \sum_{u=1}^{U} \delta(z - uL) - \sigma_D \right] \tag{13}$$

The third order deformation equation can be written as:

$$\varphi_3 = \iint R(\mu_2) \, dz^2 \tag{14}$$

Substituting the value of $R(\mu_2)$ in Eq. (14), the value of φ_3 becomes:

$$\varphi_3 = \frac{12\pi e}{\epsilon} \sigma_D \frac{Z^2}{2} - \frac{4\pi e}{\epsilon} e_{QD} \langle N \rangle Uz \tag{15}$$

The total surface potential can be obtained by adding all the three deformation equations i.e.:

$$\varphi = \varphi_1 + \varphi_2 + \varphi_3 \tag{16}$$

$$\varphi = -\frac{4\pi e}{\epsilon} \left[e_{QD} \langle N \rangle Uz - \sigma_D \frac{Z^2}{2} \right] + \frac{8\pi e}{\epsilon} \sigma_D \frac{Z^2}{2} - \frac{4\pi e}{\epsilon} e_{QD} \langle N \rangle Uz + \frac{8\pi e}{\epsilon} \sigma_D \frac{Z^2}{2} - \frac{4\pi e}{\epsilon} e_{QD} \langle N \rangle Uz + \frac{4\pi e}{\epsilon} \sigma_D \frac{Z^2}{2} \tag{17}$$

The value of surface potential can be reduced to:

$$\varphi = \frac{24\pi e}{\epsilon} \sigma_D \frac{Z^2}{2} - \frac{12\pi e}{\epsilon} e_{QD} \langle N \rangle Uz \tag{18}$$

By applying the boundary condition, the value of φ becomes:

$$\varphi = \frac{V}{U+1} + \frac{12\pi e}{\epsilon} L^2 \left[\sigma_D (U + 1) - e_{QD} \langle N \rangle \frac{U}{L} \right] \tag{19}$$

The vertical coupling of QD layers reduces the inhomogeneties of QD ensemble. It increases the dark current of the device and the charge carriers can tunnel through different QD layers more easily. The value of $< N_k >$ can be obtained from a balance relation for emission and capture of QDs.
The capture probability is given as:

$$R_P = R_{UC} \frac{<N> - <N_K>}{<N>} \exp\left[\frac{-q^2 <N>}{CKT} \right] \tag{20}$$

where,
R_P = The capture probability
R_{UC} = The capture probability of uncharged QDs close to 1
$< N >$ = The maximum number of electrons that can occupy each QD
C = The capacitance of the QD
K = The Boltzmann constant
T = The temperature
$< N_K >$ = The potential distribution in the QD layer as a function of average number of electrons in each QD

The rate of thermionic emission is given as γ:

$$\gamma = \gamma_0 \exp\left(-\frac{E_{ie}}{KT} \right) \exp\left[\frac{\pi h^2 <N>}{mKT} \right] \tag{21}$$

where, E_{ie} is the ionization energy of ground state in QDs, m is the mass of an electron and h is the plank's constant. The total equation equates the rate of electron capture and the electron emission from QDs is:

$$j_c = \frac{q e_{QD}}{R_P} \gamma_{th} \tag{22}$$

where,
q : The charge of an electron
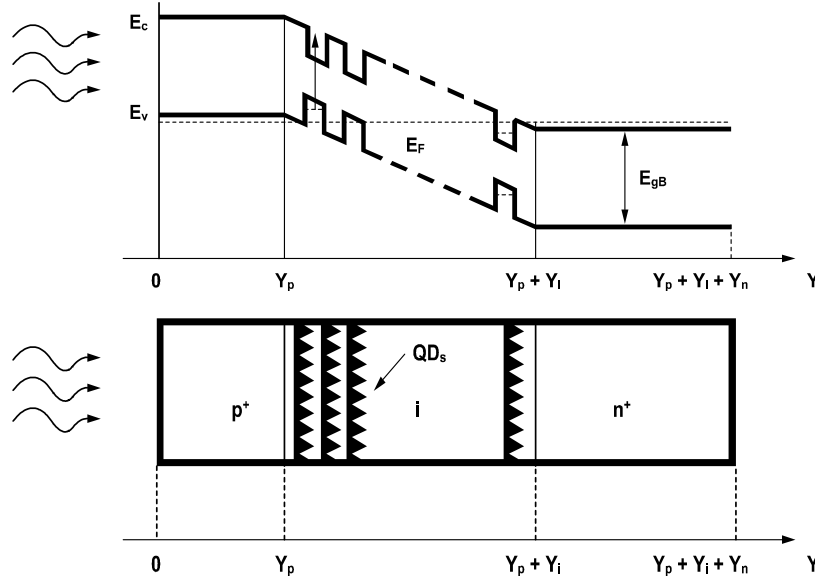e_{QD} : The density of the QD

Fig. 2: Energy band diagram and schematic view of QD solar cell

The energy of the proposed QD model can be given by the Schrodinger equation as:

$$-\frac{h^2}{2m} s_t \Delta^2 \psi + q\varphi(x,y,z)\psi(x,y,z) = E\psi(x,y,z) \tag{23}$$

where, h is the Planks constant, m is the mass of the electron, q is the electron charge, E is the energy, s_t is the strain and ψ is the wave function. To meet the desired boundary condition the value of ψ becomes:

$$\psi = 2iA\sin(\propto_z z)\, e^{i(\propto_x x + \propto_Y Y)} \tag{24}$$

And the value of $\propto_x$, $\propto_y$ and $\propto_z$:

$\propto_z = \frac{n_z \pi}{2(K+1)L}$, ψ gets the maximum value:

$$\propto_x = \frac{n_x \pi}{2L} \text{ and } \propto_y = \frac{n_y \pi}{2L} \tag{25}$$

By applying the boundary condition, the Schrodinger equation becomes:

$$\frac{h^2}{2m} s_t [\propto_x{}^2 + \propto_y{}^2 + \propto_z{}^2]\psi + q\varphi(x,y,z)\psi(x,y,z) = E\psi(x,y,z) \tag{26}$$

The energy of the QD has been obtained as:

$$E = \frac{h^2\pi^2}{8mL^2} s_t \left[n_x{}^2 + n_y{}^2 + \frac{n_z{}^2}{(U+1)^2} \right] + q[\frac{V}{U+1} + \frac{12\pi e}{\epsilon} L^2 [\sigma_D(U+1) - e_{QD}\langle N\rangle \frac{U}{L}] \tag{27}$$

The dark current flowing through the QD plays an important role in limiting the performance of the device. The dark current with respect to density J_D can be written as:

$$J_D = j_m e_{QD} \int_0^\infty \exp\left[E\varphi/K_B T\right] \mathrm{d}r^2 \tag{28}$$

where,
j_m = The maximum current density
φ = The surface potential
E = The Eigen energy:

$$r^2 = x^2 + y^2$$

$$J_m = j_m e_{QD} \exp\left[\frac{n^2\pi^2 s_t}{8mL^2} + q\left(\frac{V+V_D(U+1)}{(U+1)2K_B T}\right)\right] \exp\left[\frac{V+V_D(N+1)}{(U+1)}\right] \tag{29}$$

where,

$$\gamma^2 = \left[n_x{}^2 + n_y{}^2 + \frac{n_z{}^2}{(U+1)^2} \right]\Big/ K_B T \tag{30}$$

$$V_D = \frac{12\pi e}{\epsilon} L^2 [\sigma_D(U+1) - e_{QD}\langle N\rangle \frac{U}{L}] \tag{31}$$

Using Eq. (29), the dark current can be estimated for various applied voltage, QD density, length of the QD layer, number of QD layer and temperature.

The schematic view of QD solar cell and energy band structure is shown in Fig. 2. The model shows multi QD layers in the intrinsic region. The effective absorption for band gap occurs in the bottom level confined states. The p[+] type layer lies in the level between $0 \leq Y \leq Y_p$, intrinsic layer with QDs lies in the band levels between $Y_p \leq Y \leq Y_p + Y_i$ and n[+] type layer lies in the range between $Y_p + Y_i \leq Y \leq Y_p + Y_i + Y_n$ where the

depletion layer in p- and n-layers are neglected. i.e., $N_k^{i,j} = \langle N_K \rangle$ where i, j are in plane indices and k is the index of QD layer.

The charges of different layers of the QD remains the same and hence the average number of electrons $\langle u_k \rangle$ with k^{th} QD layers is given by the index u = 1, 2, 3, 4.....U, where U is the number of QD layers. The photovoltaic energy conversion is characterized by the important processes like photon absorption, carrier relaxation and recombination distinguished by Shockley-Read-Hall model (Movla *et al.*, 2010).

The capture of an electron by QDs from adjacent barrier regions is given as:

$$QD_C = c_r f(z,u) S_d (1 - p_n^u) \qquad (32)$$

The escape of electrons from QDs of interested layer is given as:

$$QD_e = e_r S_d p_n^u \qquad (33)$$

The recombination in QDs is given as:

$$QD_r = r_r S_d (p_n^u - p_{n0}) \qquad (34)$$

The optical generation in QDs is:

$$QD_g = o_r S_d (1 - p_n^u) \qquad (35)$$

where c_r, e_r, r_r and o_r are the capture, escape, recombination and generation coefficients and depends on the dot filling and QD layer position within the i region. The coefficients are given by the equations:

$$c_r = \frac{1}{V_D \zeta_{cp}}; \; e_r = d_1 c_r; \; r_r = \frac{1}{\zeta_{rc}}; \; o_r = \frac{1}{\zeta_{og}} \qquad (36)$$

Here V_D and d_1 are QD volume concentration and density of free electrons. The capture rate is also depicted by $c_r = \sigma_{QD} v_t$, σ_{QD} is the QD electron capture cross sectional area and v_t is the average thermal velocity of electrons at room temperature. ζ_{og} is the optical generation life time and ζ_{rc} is the recombination life time dependence on electric field E_F. p_n^u is the average of non-equilibrium population of QDs in the Uth layer, p_{n0} is the equilibrium of Fermi-Dirac occupation probability and f (z, u) is the density of free electrons at the frontal surface of Uth layer with position of $z_u = (u - 1)d$.

Under steady state operation, the following condition is applied:

$$(QD_C - QD_e) + (QD_r - QD_g) = 0 \qquad (37)$$

The recombination rate QD_r and optical generation rate QD_g becomes $QD_r = QD_g = 0$ under dark condition and hence the above equation can be changed as:

$$c_r d_0 (1 - p_{n0}) - e_r p_{n0} = 0 \qquad (38)$$

where, the equilibrium density of electrons, population probability of QDs and free density of electrons are given by the equations:

$$d_0 = D_c \exp \left(\frac{E_f - E_c}{kT} \right) \qquad (39)$$

$$p_{n0} = \left[1 + exp \left(\frac{E_n - E_f}{kT} \right) \right]^{-1} \qquad (40)$$

$$d_1 = D_c exp \left(-\frac{E_c - E_n}{kT} \right) \qquad (41)$$

where, the coefficient c_r can be written:

$$e_r = n_1 c_r \qquad (42)$$

And E_c, E_f, kT, E_n are conduction band edge, Fermi energy, thermal energy, confinement energy in the QD respectively and D_c is the effective density state in conduction band of QDs.

The population factor p_n^u can be obtained as:

$$p_n^u = \frac{-c_r f(z,u) + r_r p_{n0} + o_r}{-c_r [f(z,u) + d_1] + r_r + o_r} \qquad (43)$$

The effective surface recombination rate on the plane of Uth QD's layer is defined as:

$$U_s^u = QD_C - QD_e \qquad (44)$$

The total effective surface recombination rate U_{tot}^u is the total possible recombination paths of QD solar cell in non-equilibrium state and it is the sum of effective surface recombination rate U_s^u and effective interband recombination rate U_{it}^u:

$$U_{tot}^u = U_s^u + U_{it}^u \qquad (45)$$

The effective surface recombination rate is defined by:

$$U_s^u = c_r S_d \frac{[f(z,u)(d_1 + r_r - r_r p_{n0} + c_r d_1) - d_1 r_r p_{n0} - o_r]}{-c_r [f(z,u) + d_1] + r_r + o_r} \qquad (46)$$

The inter-band transition is considered for the evaluation of QD carrier generation or recombination and carrier dynamics. The effective surface recombination rate u, U_{it}^u is given as:

$$U_{it}^u = S_d \left[\frac{(c_r [f(z,u)] + r_r p_{n0} + o_r)(r_r + o_r)}{c_r [f(z,u)] + e_r + r_r + o_r} - r_r p_{n0} - o_r \right] \qquad (47)$$

The total surface recombination rate U_{tot}^u can have positive or negative values. The QDs behave as recombination centers for positive values and as

generation centers for negative values. Such behavior strongly depends on the movement of free electrons and proper balance should be obtained between the transition rate U_s^u, U_{it}^u. The total generated photocurrent in i-region is calculated self-consistently by taking into account the existence of QDs through the total surface recombination rates U_{tot}^u and solving the current continuity equation for inter-layer regions.

The electron current density of the QD consists of two components, namely the drift current component as main part and diffusion current component due to recombination in the inter-layer region as the negligible part are given by the relations:

$$j_n = q\mu_m E_F + qD_d \nabla_d \tag{48}$$

$$-\mu_m E_F \frac{df(z,u)}{dz} = F(\lambda)\alpha(\lambda)\exp\left[-\alpha(\lambda)\right] \tag{49}$$

where, q, μ_m, $f(z,u)$ and E_F are the electron charge, electron mobility of barrier region, density of free electrons in the inter-dot region and electric field respectively. Light absorption coefficient with wavelength dependency and flux of incident light $\alpha(\lambda)$ = $\sigma_{opt} e_{QD}$, where σ_{opt} is the optical absorption cross section.

The photocurrent is calculated with free electron density n (z, 1) in the first inter dot region during the first interval $0 \le z \le d$ for the incident light of wavelength λ and flux F (λ) via the equation:

$$\mu_m E_F \frac{df(z,1)}{dz} F = (\lambda)\alpha(\lambda)\exp\left[-\alpha(\lambda)z\right] \tag{50}$$

Solving Eq. (50) with respect to $f(z,1)$ and defining $L_d = 2D_d/\mu_m E$ as electron diffusion length, we get:

$$f(z,1) = A + \frac{L_d}{2D_d} F(\lambda)\exp\left[-\alpha(\lambda)z\right] \tag{51}$$

where, D_d is the diffusion coefficient. Constant A is calculated by considering the boundary condition arising from adjoining the p-emitter to i-region:

$$q\frac{2D_d}{L_d}f(z=0,1) = j_p^0 - qU_s^1 \tag{52}$$

Here, j_p^0 is the electron current density at the edge of p-emitter region in the first inter dot region and consequently, for other layers it can be written as:

$$q\frac{2D_d}{L_d}f(z,u) = j_p^{u-1} - qU_s^u \tag{53}$$

The total collected photocurrent at the end of Uth layer from the intrinsic region, including photocurrents generated in both inter-dot regions and QD layers is formulated by the equation:

$$J_{Ph} = J_D + qF(\lambda)(1 - \exp(-\alpha(\lambda)d)) \tag{54}$$

The first term is generated from QD layers under dark condition and the second term is created by the inter-dot region.

The spectral response of a solar cell is defined as:

$$R(\lambda) = \frac{J_{Ph}(\lambda)}{E(\lambda)} \tag{55}$$

where, $J_{Ph}(\lambda)$ is the photocurrent density of illuminated cell with irradiance $E(\lambda)$.

The model of solar spectrum described by black body curve corresponding to a temperature T = 5760 K and incident solar flux on the cell surface under 1 Sun, 1.5 AM condition are considered. To obtain the efficiency of solar cell structure, the standard superposition model is considered for modeling and the efficiency depends on various parameters at maximum power point. The efficiency of illuminated solar cell is calculated using the expression:

$$\eta = \frac{V_{oc} J_{sc} FF}{P_{in}} \tag{56}$$

where,
η = The efficiency of the solar cell
V_{oc} = The open circuit voltage
J_{sc} = The short circuit current
FF = The fill factor
P_{in} = 116 mW/cm^2 is the input solar intensity or power density of the incoming solar radiation at 1 Sun, 1.5 AM condition

RESULTS AND DISCUSSION

The 3D Poisson's Eq. (1) using the boundary conditions (2) is solved numerically using Homotopy analysis to determine the surface potential for various fixed values of applied voltages and assumed electron parameters like length, number of electrons and number of layers of QD. The value of the surface potential is given to the 3D Schrodinger Eq. (23). The 3D Schrodinger equation is solved by using the boundary conditions and the exact value of eigen energy is calculated. The Integro-Derivative approach is adopted to solve the surface potential φ with the available boundary conditions. The surface potential and eigen energy are calculated numerically at consequent points and the device characteristics are estimated.

The ranges and values of the parameters used for the numerical computation of the surface potential and device energy to establish the numerical model using Homotopy analysis and its utilization in QDSC are given in Table 1. It is found that the results achieved through the proposed model navigate the QDSC performance for a given spectrum of wavelength.

Table 1: Parameters and constant values

Parameters	Value
Dielectric constant, ε	8.854×10^{-12} Fm^{-1}
Density of the QD, e_{QD}	0.2-1.4×10^{14} m^{-2}
No. of electrons in the QD layer, N	5-1000
Dirac delta function, δ	1
Donor concentration, σ_D	10^{18} m^{-3}
Length of the QD layer, L	5-50 nm
Applied voltage, V	0.2-1.2 V
No. of QD layers, U	5-50
Capture probability of uncharged QDs, R_{UC}	1
Temperature, T	50-500 K
Dark current saturation density, j_o	3.29×10^3 m^2
Ideality factor, n	1-2
Shunt resistance, R_{sh}	1.2×10^5 $\Omega.$cm^2
QD volume concentration V_D	10^{17}-10^{20} cm^3
Average thermal velocity of electrons at room temperature, v_t	10^7 cm/sec
Optical generation life time, ζ_{og}	1-10 nsec
Recombination life time, ζ_{rc}	10-1000 nsec
ζ_{cp}, capture time	50-300 psec
Optical absorption cross section, σ_{opt}	10^{10}-10^{11} cm^2
Electron diffusion length, L_d	590 μm
Diffusion coefficient, D_d	200 cm/sec
Constant A is calculated by considering the boundary condition arising from adjoining the p-emitter to the i-region	$3.5*10^{21}$
j_p^0 is the electron current density at the edge of p-emitter region in the first inter dot region	22 mA/cm^2

Table 2: Comparison of surface potential between the QD layers for V = 1.1 V

No. of QD layer	Surface potential (V)	Potential difference (V) between QD layer
25	0.0423	0.0264
35	0.0306	0.0117
75	0.0145	0.0161
100	0.0109	0.0036
250	0.0044	0.0065
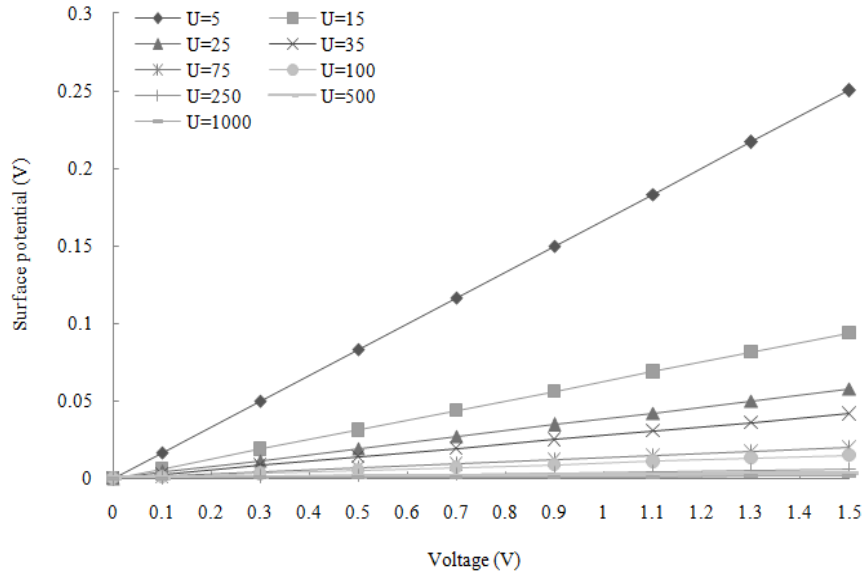
Fig. 3: 3D surface potential variation with applied voltage for different QD layers, $e_{QD} = 1.3\times10^{14}$ m^{-2}, N = 10 and L = 10 nm

Figure 3 shows the variation of surface potential of the quantum dots with applied voltage including the quantum mechanical effects. The surface potential is calculated for different voltage values. It is found that the surface potential increases linearly with respect to applied voltage and conversely the potential decreases with the increasing QD layers. For example, at V = 1.3 V, when the number of QD layers changes from U = 5 to U = 500, the surface potential gets rapidly reduced to 0.0026 V. This is due to the fact that the reduced carrier density experiences the Fermi level to bend from the energy band where the majority carriers reside and this increases the surface potential. The change in surface potential indicates the capability of minority carriers to reach the surface.

Table 2 shows the variation in surface potential due to change in the number of QD layer. For example, the potential difference between the QD layers is 0.0379 V,
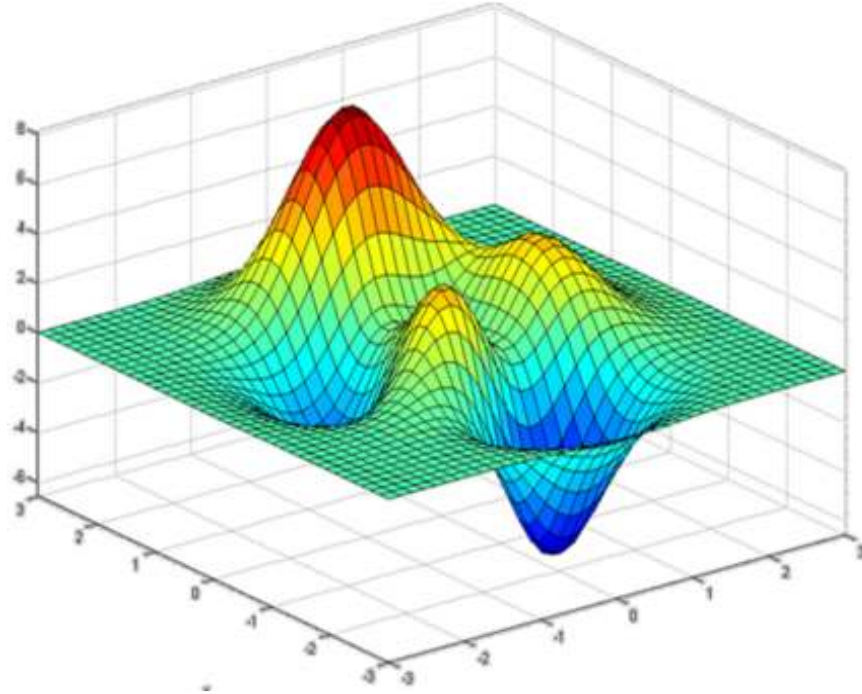
Fig. 4: Variation of three dimensional surface potential with applied voltage
x: Applied voltage (V); y: Surface potential (V); z: Number of QD layers
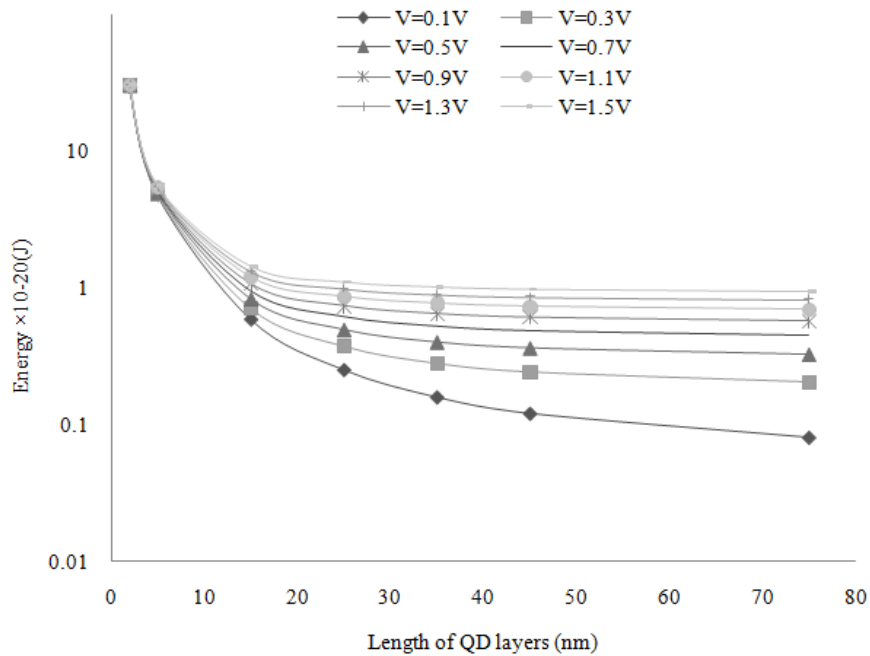

Fig. 5: Variation of energy with length of QD layers for various applied voltages

when the number of QD layer changes from 25 to 250 for the applied voltage of V = 1.1 V.

Figure 4 shows the surface potential profile of the quantum dot including quantum mechanical effect obtained using homotopy analysis. It is found that the surface potential increases linearly with respect to applied voltage. However, the potential decreases for higher number of QD layers. The change in the surface potential is significant with the number of QDs for an applied voltage. This may be due to reduced carrier density which makes the Fermi level to bend from the electronic energy band where the majority carriers reside and this improves the surface potential. The change in surface potential indicates the ability of

minority carriers to reach the surface. The surface potential decreases exponentially with the increasing of QD layers. At high L values, the larger inter gap between the QD leads to reduced coupling between the QDs and makes the surface potential independent of the length of the QD layer.

Figure 5 shows the comparison of length of the QD layers with energy for a nano scale QD with N = 10 and $e_{QD} = 1.3 \times 10^{14}$ m^{-2}. The simulated result shows that the energy decreases rapidly as the length of the QD layer increases from 5 to 50 nm. It seems that the rapid decrease in energy level is due to the fact that the carrier density near the collector end decreases gradually. The change in energy is significant with the length of QDs for an applied voltage and it is due to the decrease in the average number of carriers inside the QDs. The energy experiences a gradual drop with the

higher number of QD layers leading to the recombination of electrons. Hence, with the increasing QD layers, the active volume of the QD layers increases and the energy decreases.

The variation of dark current with QD density for various applied voltages, U = 10, L = 10 nm and T = 25 K is obtained and shown in Fig. 6. It is found that the dark current decreases with increase in density and drops to minimum and maintains saturation for high quantum density values. The low energy electrons and reduced number of electrons in the QDs transits optically from the ground state to the continuum state. The low repulsive potential of the carriers in the QD causes increase in capture probability and reduces the dark current.

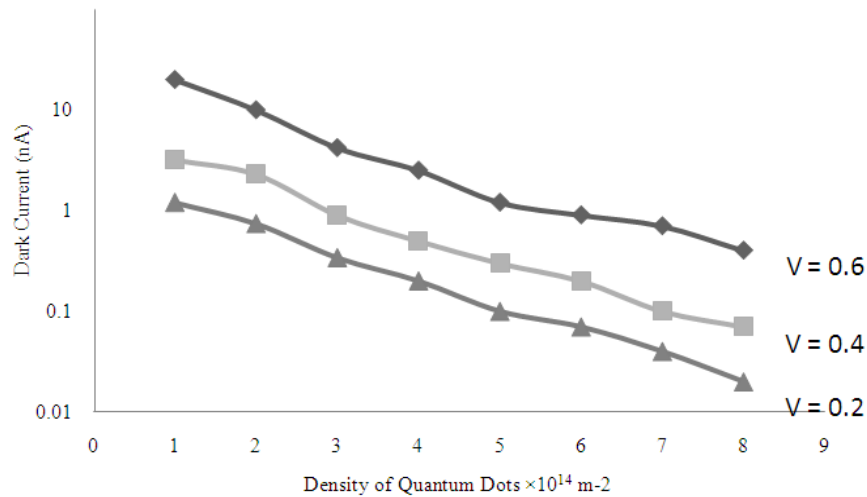Figure 7 to 9 shows the effective surface recombination rate U_s^u, effective inter band

Fig. 6: Dark current variation with QD density for different voltages
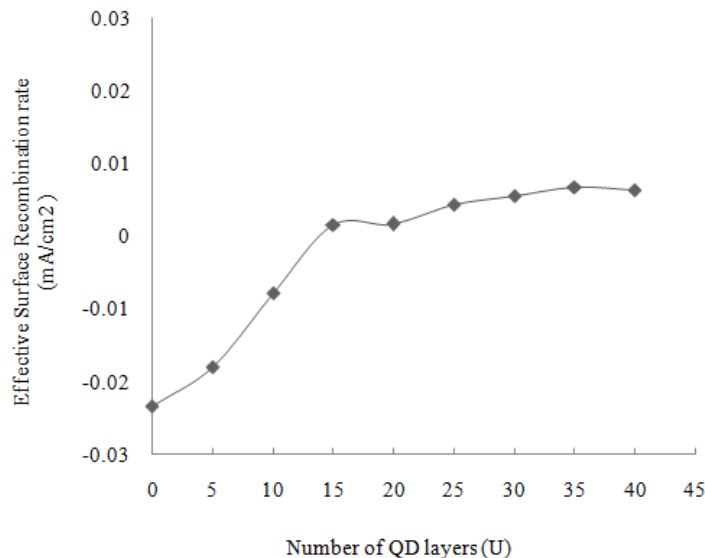

Fig. 7: Variation of effective surface recombination rate U_s^u with number of QD layers U
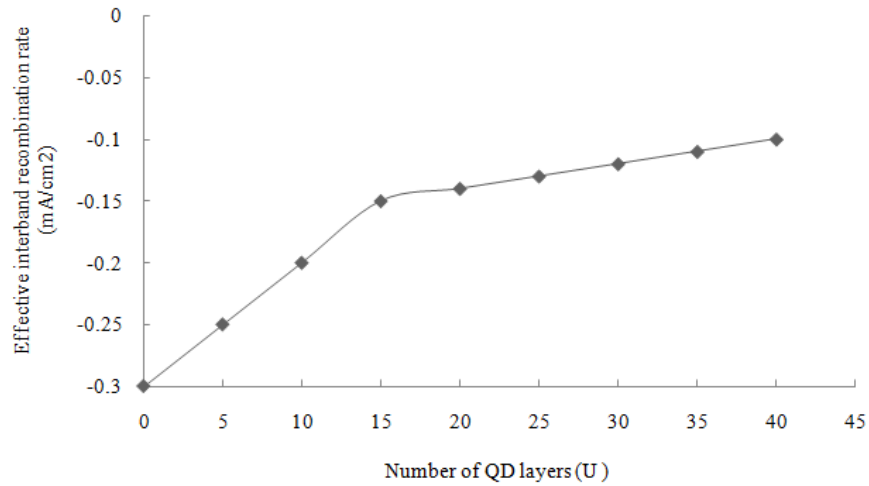
Fig. 8: Variation of effective inter band recombination rate U_{it}^u with number of QD layers U
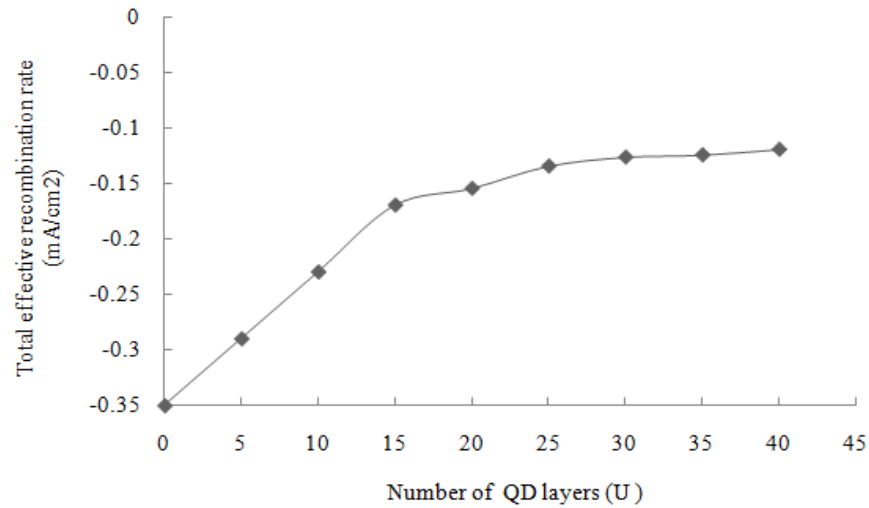

Fig. 9: Variation of total surface recombination rate U_{tot}^u with number of QD layers U

recombination rate U_{it}^u, effective total surface recombination rate U_{tot}^u and Fig. 10 shows the photocurrent density as a function of number of QD layers U for $\zeta_{rc} = 10$ nsec, $\zeta_{og} = 10$ msec, $\zeta_{cp} = 1$ nsec, T = 80 K, $e_{QD} = 1.3 \times 10^{14}$ m^{-2}, V = 0.7 V, L = 10 nm, $\lambda = 500$ nm. The photocurrent density increases with the increase in QD layers and QDs behave as generation centers due to the negative effective recombination rate. The photocurrent density follows the changes of surface recombination rate and it increases for U≤15 and it remains standstill for U≥15 due to the positive recombination rates. The QDs behave like recombination centers due to localized carrier concentration. It is observed that the optimal and minimal number of QD layers i.e., U = 15 layers are enough to generate maximum photocurrent for lesser recombination life time. It is also found that the generation carrier centers decrease for increased QD

layers and does not contribute to conversion efficiency. The short circuit current density $J_{sc} = 51.21$ mA/cm^{-2} and open circuit voltage $V_{oc} = 0.69$ V and conversion efficiency $\eta = 77.4\%$ are obtained. The current density increases due to the enlargement of intrinsic region and bundled QD layers absorb the low energy photons.

The fill factor of 80.56 is obtained at temperature T = 80 K, spectral irradiance of 500 W/m^2 and it enhances the short circuit current $J_{SC} = 51.21$ mA/cm^{-2} without significant loss in the open circuit voltage $V_{oc} = 0.69$ V with an ideality factor n = 1. The open circuit voltage shows considerable decrease compared with other models. The increase in the photo generation level due to strong carrier confinement in the QDs and inhomogeneous broadening of the absorption spectra corresponding to different electron-hole transition levels increase the fill factor contributing to the increased efficiency $\eta = 77.4\%$.
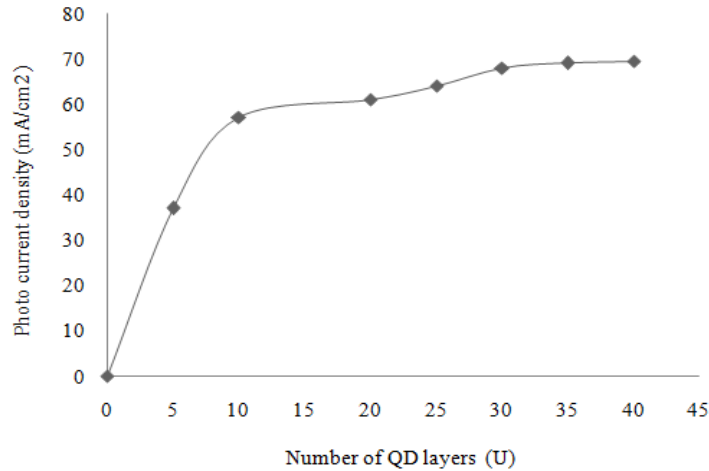
Fig. 10: Variation of photocurrent density with number of QD layers U
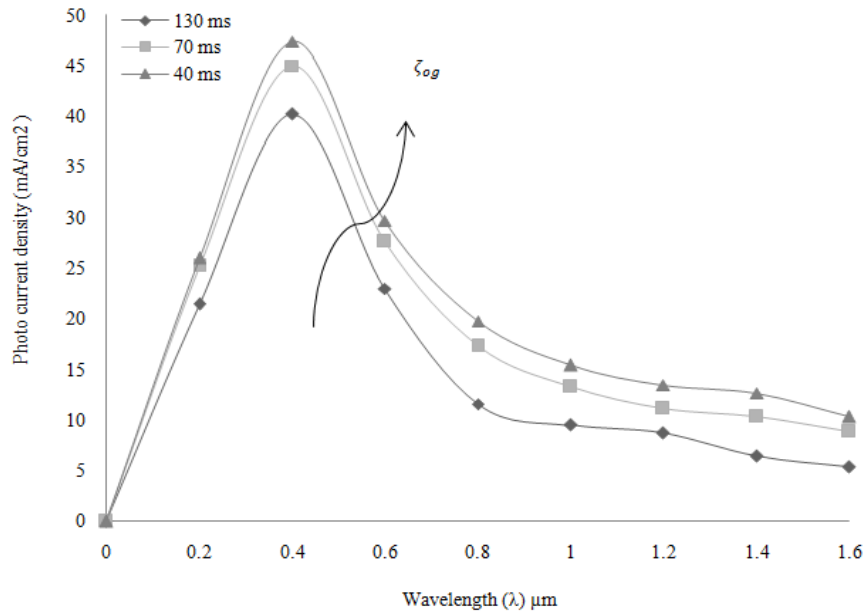

Fig. 11: Variation of photocurrent density vs. wavelength λ for different ζog values

Figure 11 shows the variation of photocurrent density with wavelength λ for different optical generation life time, ζog at ζ_{rc} = 10 nsec, e_{QD} = 1.3× 10^{14} m^{-2}, U = 15, T = 80 K, V = 1.1 V, L = 10 nm, V_D = 10^{17} cm^{-3} 10^{17}. The photocurrent density reaches the maximum at 500 nm and decreases at a nominal rate in the optical range. The photocurrent drops from 34 mA/cm^2 at ζog = 40 msec to 29 mA/cm^2 at ζog = 130 ms when the light intensity is λ = 500 nm due to the higher carrier concentration at high optical generation rates. Hence QDs behave as recombination centers instead of generation centers at higher ζog.

Figure 12 shows the variation of photocurrent density with light intensity for different QD densities and other constant parameters ζ_{rc} = 10 nsec, ζ_{og} = 55 msec, T = 80 K, V = 1.1 V, L = 10 nm , V_D = 10^{17} cm^{-3}.

It is found that the maximum photocurrent is obtained at near 450-550 nm in the close proximity of optical range. The maxima photocurrent can be shifted to the optical range by introducing the additional QD layers called luminescent concentrators. The photocurrent density is found to be maximum at low QD density values e_{QD} = 1.1*10^{14} m^{-2} and decreases for higher QD density values due to the increased inter-gap area and electron hole recombination.

Figure 13 shows the variation of photocurrent with applied voltage for various QD densities at ζ_{og} = 55 nsec, ζ_{rc} = 10 nsec, T = 80 K, T_1 = 5760 K, L = 10 nm, U = 15. The photocurrent increases steadily with the applied voltage for the fixed values of ζog and ζr. It is found that the photocurrent increases with low e_{QD} values. The efficiency is around 77.4% at
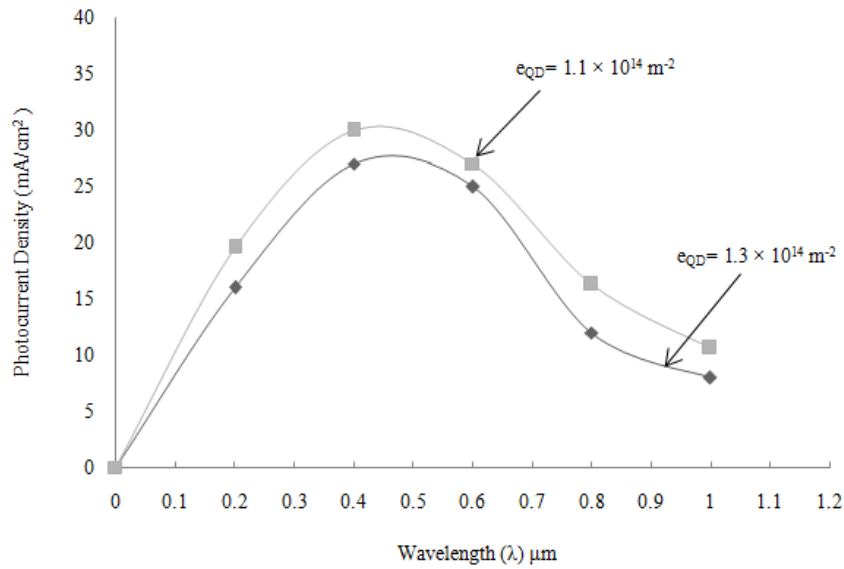
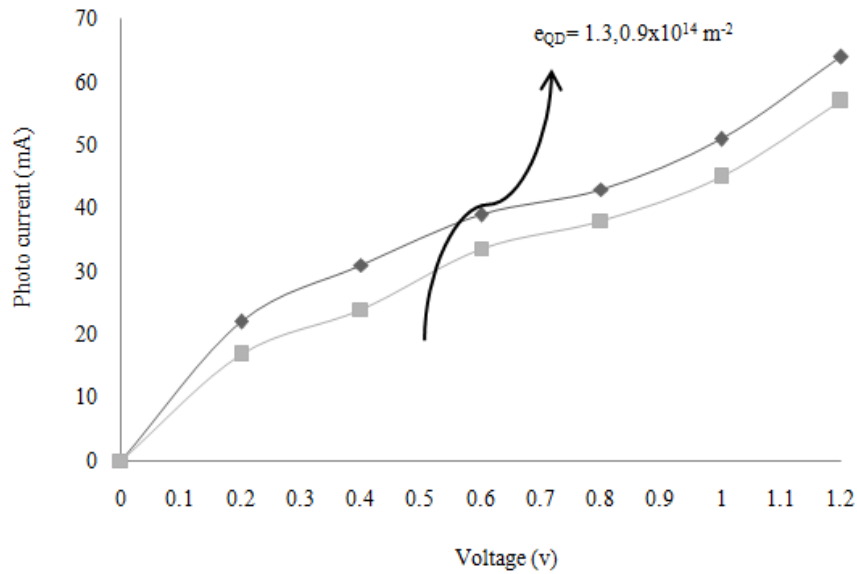Fig. 12: Photocurrent density vs. wavelength λ at different e_{QD} values

Fig. 13: Photocurrent with applied voltage characteristics for various QD

$e_{QD} = 0.7 \times 10^{14}$ m^{-2}. The small QD density influences the interaction of free holes and free electrons and makes the QD act as generation centers and increases the electron mobility. The recombination at lower density and temperature make the photocarriers to be electric field and voltage dependent resulting in high photocurrent values.

Figure 14 shows the variation of the photocurrent with applied voltage for different QD layers U at $\zeta_{og} = 55$ nsec, $\zeta_{rc} = 10$ nsec, $e_{QD} = 1.3 \times 10^{14}$ m^{-2}, T = 80 K, L = 10 nm. The photocurrent increases with applied voltage consistently along with the increasing QD layers. For example, the photocurrent straightly increases from 38 to 45 mA for the decrease of QD

layers U = 25 to 15 when the applied voltage is 1.0 V. It was inferred that the photocurrent increases with the increase in QD layers up to U = 15 due to its behavior as generation centers and it slows down at U≥15 due to the positive value of the surface recombination rate and QD layers act as recombination centers. The photocurrent is voltage dependent and as the carrier concentration increases for increasing QD layers, surface recombination rate decreases simultaneously by reducing the generation centers. The intrinsic layer becomes thicker due to the addition of QD layers and it leads to the recombination of carriers. Hence photocurrent does not show promising increase for further QD layer additions.
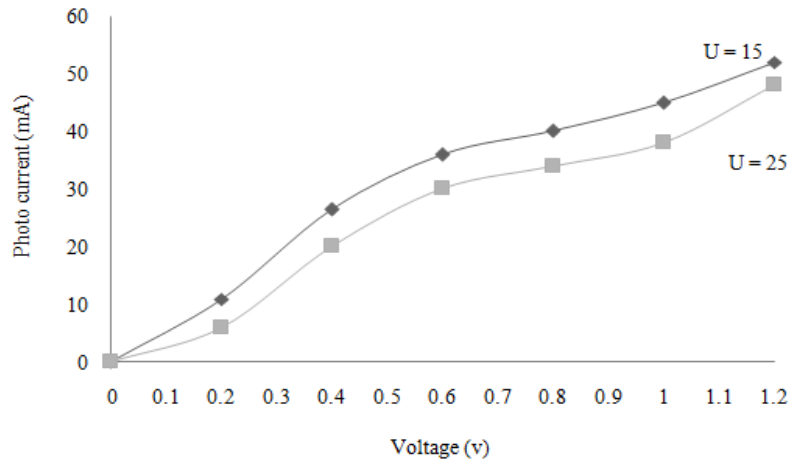
Fig. 14: Photocurrent as a function of applied voltage at different QD layers U
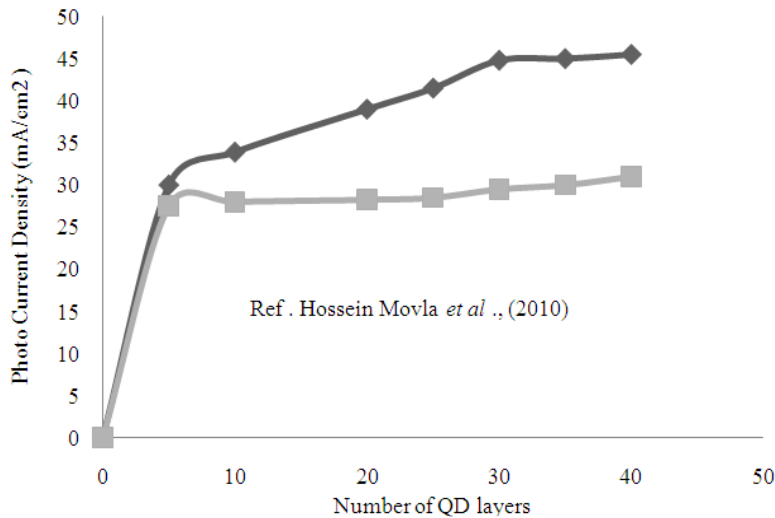

Fig. 15: Variation of photocurrent density with number of QD layers at ζ_{rc} = 1 psec

The variation of photocurrent with number of QD layers U using Homotopy analysis is obtained in Fig. 15 and it shows a good agreement with the experimental values (Movla *et al*., 2010). The photocurrent increases with the number of QD layers incorporated and reaches its maxima with QD layers U = 15. It is inferred that the QDs in active region, especially small sized QDs near the anode and large sized QDs near the cathode, QD concentration, barrier thickness leads to the increase in the photocurrent density.

It is also observed that the photocurrent obtained by the developed model is high compared with the work of Movla *et al*. (2010). The developed model based on Homotopy analysis provides flexible, self-consistent solutions to 3D Poisson and Schrodinger equations. The convergence control parameter enforcing convergence to the series solution made the model to achieve high values of photocurrent for the prescribed parameters.

CONCLUSION

The homotopy analysis approach based numerical model of QD solar cell under dark and incident solar energy conditions are presented. The semi analytical approach enhances the solution of 3D Poisson and Schrodinger equations by splitting the non-linear parameters into linear parameters. The developed model has concluded that based on the QDSC parameters and available optimum QD layers of U = 15, maximum photocurrent was obtained around 500 nm wavelength spectrum. The effective recombination rates and photocurrent shows promising results and are compared with the experimental results for validations. The photocurrent of 65 mA and conversion efficiency around 77.4% was evident without significant loss in the open circuit voltage for the incident solar energy under 1 Sun, 1.5 AM condition. It is concluded that the developed QDSC

model using Homotopy analysis can be extended to practical implementations.

ACKNOWLEDGMENT

REFERENCES

Al-Daby, G., M. Dhamrin and K. Kamisako, 2010. Use of Green's Function method for developing a 3 D mathematical model for studying the photo response of fibrously grained polycrystalline Silicon Solar Cell. Proceeding of 5th World Conference on Photovoltaic Energy Conversion, Spain, pp: 480-483.

Aly, A.E.M. and A. Nasr, 2014. Theoretical study of one-intermediate band quantum dot solar cell. Int. J. Photoenergy, Article ID 904104, pp: 10.

Aroutiounian, V., S. Petrosyana and A. Khachatryan, 2001. Photocurrent of quantum dot p-i-n solar cells. J. Appl. Phys., 89(4): 2268-2271.

Battacharya, P., A.D. Stiff Roberts, S. Krishna and S. Kennerly, 2002. Quantum dot infrared detectors and sources. Int. J. High Speed Electron. Syst., 12(4): 969-994.

Datta, S., 2000. Nano scale device modeling: The Green's function method. J. Superlatt. Microstruct., 28(4): 253-278.

Eshaghi Gorji, N., M.H. Zandi, M. Houshmand and M. Shokri, 2012. Transition and recombination rates in intermediate band solar cells. Scientia Iranica, 19(3): 806-811.

Fariborzi, M.A. and A. Fallahzadeh, 2012. On the convergence of the Homotopy analysis method for solving the schrodinger equation. J. Basic Appl. Sci. Res., 2(6): 6076-6083.

Fonseca, L.R.C., J.L. Jimenez, J.P. Leburton and R.M. Martin, 1998. Self consistent calculation of the electronic structure and electron-electron interaction in self-assembled In As-GaAs quantum dot structures. Phys. Rev. B, 57: 4017- 4026.

Hossein Zadeh, H, H. Jafari and S.M. Karimi, 2010. Homotopy analysis method for solving integral and integro differential equations. Int. J. Res. Rev. Appl. Sci., 2(2): 140-144.

Madheswaran, M. and K.R. Kavitha, 2013. 3D numerical modeling of quantum dot using homotopy analysis. J. Comput. Electron., 12(3): 526-537.

Marti, A., L. Cuadra and A. Luque, 2002. Design constraints of the quantum dot intermediate band solar cell. Physica E, Low-dimensional Syst. Nanostruct., 14(1): 150-157.

Melnikov, D.V., J. Kim, L.X. Zhang and J.P. Leburton, 2005. Three dimensional self-consistent modeling of spin-qubit quantum dot devices. IEEE Proceed. Circ. Dev. Syst., 152(4): 377-384.

Milicic, S.N., F. Badrieh, D. Vasileska, A. Gunther and S.M. Goodnick, 2000. 3D modeling of silicon quantum dots. Superlatt. Microstruct., 27(5/6): 377-382.

Movla, H., F. Sohrabi, J. Fathi, H. Babaei, A. Nikniazi, K. Khalili and N. Es'haghiGorji, 2010. Photocurrent and surface recombination mechanisms in the In_xGa1-_xN/GaN different-sized quantum dot solar cells. Turk J. Phys., 34: 97-106.

Nasr, A., 2013. Theoretical study of the photocurrent performance into quantum dot solar cells. Optics Laser Technol., 48: 135-140.

Semichaevsky, A.V. and H.T. Johnson, 2013. Carrier transport in quantum dot solar cell using semi classical and quantum mechanical model. Solar Energ. Mater. Solar Cells, 108: 189-199.

Sheng, W. and J.P. Leburton, 2002. Anomalous quantum-confined stark effects in stacked InAs/GaAs self-assembled quantum dots. Phys. Rev. Lett., 88(16): 167401:1-4.

Yildirim, S., 2008. Exact and numerical solutions of poisson equation for electrostatic potential problems. Mathem. Prob. Eng., 2008, Article ID 578723, pp: 1-11.